Theoretical Chemistry Accounts (2018) 137:68
https://doi.org/10.1007/s00214-018-2245-9

REGULAR ARTICLE

Insights into the bonding between tributylphosphine chalcogenides and zinc(II)

Zied Gouid[1,2] · Ridha Ben Said[1] · Med Abderrahmane Sanhoury[3,4] · Salima Boughdiri[1] · Muthuramalingam Prakash[5] · Roberto Linguerri[2] · Majdi Hochlaf[2]

Received: 30 January 2018 / Accepted: 11 April 2018 / Published online: 19 April 2018

Abstract
We present a first-principles systematic study on the bonding and structure of the complexes between zinc(II) chloride and tributylphosphine chalcogenides, n-Bu_3PE (E = O, S, Se). These investigations are carried out within the framework of the density functional theory with and without considering the dispersion corrections evaluated at the GD3 level. Inspection of the calculated binding energies, orbitals, charge transfers and natural bond orbital analysis shows the importance of the interplay between σ- and π-type bonding within P–E and E–Zn in the formation of these complexes. Calculations reveal that the P–E–Zn angle goes from 120° to 90° when going from O to Se. In the complexes, the P–E bonds resemble those in the isolated PE^- diatomic anions, where an electron density excess is found on the chalcogen E whatever its nature. A bonding model for this type of organometallic complexes is proposed and discussed here for the first time.

Keywords Density functional theory · Tributylphosphine chalcogenides · Zinc complexes

1 Introduction

Tertiary phosphines (R_3P, R = organic derivative) are an important subclass of organophosphines with a wide range of applications in chemistry. For instance, they form complexes with metal ions (M) acting as catalysts and react easily with chalcogens, producing phosphine chalcogenides (R_3PE, E = O, S, Se), which exhibit high solubility and good reactivity toward different metal ions in diverse organic solvents [1–8]. Hence, a variety of phosphine chalcogenide–metal complexes were synthetized and characterized [9, 10]. Such complexes are of primary importance for a large spectrum of applications, [11–14] where mechanisms describing the formation of metal–phosphine chalcogenides (R_3PE–M) and the P–E bond cleavage are of primary importance. The control of these steps is closely connected with their industrial exploitations. This goes through the in-depth characterization of the R_3PE–M complex structures and, more specifically, of the respective P–E and E–M bond nature.

In the literature, two models are established to explain the bond formation between E and M: the σ- and π-type complex models [9]. Within the σ-type model, the interaction between R_3PE and the metal is ensured by an E lone pair donation to the metal, whereas a π donation of the P–E bond occurs in π-type complexes. Strictly speaking, a linear P–E–M bond angle is obtained in σ-type complexes, whereas a strongly bent P–E–M angle (of ~ 90°) is expected in π-type ones. Nevertheless, although the majority of phosphine oxides tend to form σ-type structures, these complexes exhibit a wide range of P–E–M angles comprised within

Electronic supplementary material The online version of this article (https://doi.org/10.1007/s00214-018-2245-9) contains supplementary material, which is available to authorized users.

✉ Roberto Linguerri
roberto.linguerri@u-pem.fr

1 Physico-Chimie des Matériaux à l'Etat Condensé, Département de Chimie, Faculté des Sciences de Tunis, Université Tunis El Manar, 2092 Tunis, Tunisia

2 Laboratoire Modélisation et Simulation Multi Echelle, MSME UMR 8208 CNRS, Université Paris-Est, 5 bd Descartes, 77454 Marne-la-Vallée, France

3 Research Unit in Materials Chemistry, Faculty of Sciences and Techniques, UNA, Nouakchott, Mauritania

4 Laboratory of Structural Organic Chemistry: Synthesis and Physicochemical Studies, Department of Chemistry, Faculty of Sciences of Tunis, University of Tunis El Manar, 2092 Tunis, Tunisia

5 Department of Chemistry, SRM Research Institute, SRM University, Kattankulathur, Tamilnadu 603203, India

these two limits, indicating that a given degree of mixing between these two types of bonding takes place invariably. Accordingly, the final structure results from the interplay between both contributions (cf., for instance, Table 7 in Refs. [9, 10]). Moreover, both types of complexes have different P–E lengths, where P–E distances are shorter within the σ-type complexes than in π-type ones. This is related to a change in the charge distribution along the P–E bond for the two types, where a P^{-}–E^{+} polarization is found in σ-type bonds and the opposite in π-types. The analysis of the P–E bond length and P–E–M bond angle is a priori sufficient to reveal the nature of the bonding in metal–phosphine chalcogenide complexes.

In the present work, first-principles methodologies are used to thoroughly investigate the complexes of $ZnCl_2$ with n-Bu_3PE (E = O, S, Se). To achieve this, we derived equilibrium structures for these systems and performed vibrational, frontier molecular orbitals (MOs), and natural bond orbital (NBO) analyses. We examined several local minima on the ground-state potential energy surface and carefully explored the configuration space near the achieved stationary points by starting new geometry optimizations from a few displaced geometries. The nature of the stationary points that were selected after this procedure was elucidated by a subsequent calculation of harmonic vibrational frequencies. Moreover, the role and effects on the molecular structures of covalent and non-covalent interactions within these complexes are examined. Prior to this, we computed the properties of the free ligands n-Bu_3PE. The complexation-induced effects on these ligands are discussed as well.

2 Equilibrium structures of tributylphosphine chalcogenides, n-Bu_3PE (E = O, S, Se)

Table 1 lists the main geometrical parameters (i.e., P=E and P–C distances and E–P–C angles) of tributylphosphine chalcogenides (n-Bu_3PE, E = O, S, Se) as optimized using the hybrid functionals M05-2X [18], PBE0 [19–21], and B3LYP [22–24] with and without considering Grimme's (DFT-D3) dispersion correction [25] as implemented in the Gaussian 09 suite of programs [26], where the atoms were described using the 6-311++G(d,p) basis set. Also, we give the values for the ν(P=E) stretching modes and the available experimental data for comparison.

For n-Bu_3PO, we compute a P=O distance of 1.500–1.505 Å, which compares favorably with the 1.489(2) Å experimental value deduced from the X-ray structure of single-crystal n-Bu_3PO [16]. The difference may be attributed to the gas phase (here) versus crystal phase [16] determinations. For P–C, we calculate a P–C

Table 1 DFT optimized main geometrical interatomic distances (in Å) and angles (in degrees) for tributylphosphine chalcogenides, n-Bu_3PE (E = O, S, Se) ligands. The atoms were described using the 6-311++G(d,p) basis set. ν(P=E) (E = O, S, Se) is the P=E anharmonic stretching frequency. [a]The full set of data is given in the supplementary material

	M05-2X	M052X+D3	PBE0	PBE0+D3	B3LYP	B3LYP+D3
n-Bu_3PO						
P=O	1.502	1.502	1.500	1.500	1.505	1.505
P–C	1.829	1.830	1.831	1.828	1.845	1.841
O–P–C	113.1	113.1	113.0	113.2	113.0	113.3
ν(P=O)	1129	1129	1138	1139	1129	1133
	1157[b]					
n-Bu_3PS						
P=S	1.975	1.973	1.966	1.965	1.981	1.979
P–C	1.833	1.835	1.836	1.826	1.852	1.847
S–P–C	113.6	113.4	113.3	113.5	113.3	113.9
ν(P=S)	566	583	585	586	573	558
	595[c]					
n-Bu_3PSe						
P=Se	2.126	2.126	2.120	2.119	2.126	2.121
P–C	1.834	1.834	1.837	1.835	1.855	1.851
Se–P–C	113.3	113.3	113.5	113.5	113.1	113.5
ν(P=Se)	496	496	494	497	505	508
	511[c]					

[a]The anharmonic frequencies are deduced from the corresponding harmonic ones after using these scaling factors: for M05-2X = 0.9470, PBE0 = 0.9592, B3LYP = 0.9662 for high frequencies and M05-2X = 0.9688, PBE0 = 0.9698, B3LYP = 0.9833 for low frequencies. Ref. [15]

[b]Experimental IR values. Ref. [16]

[c]Experimental IR values. Ref. [17]

distance of ~ 1.83 Å, which compares well with the experimental value of 1.798(2) Å [16]. For the O–P–C angle, the agreement is even more satisfactory, since the difference between the computed and measured angle is less than 0.1° [16]. As for ν(P=O), we evaluate it at 1126–1139 cm^{-1}, which is close to the IR-determined corresponding fundamental of 1153 cm^{-1} [16]. Note that B3LYP slightly overestimates the P=E and P–C bond distances and the inclusion of the dispersion effects does not significantly affect the results. The comparison between experimental and calculated data in Table 1 would confirm the accuracy of our predictions for the other ligands and complexes.

The P=E bond lengths of 1.50 Å for P=O, 1.97 Å for P=S and 2.12 Å for P=Se in the n-Bu_3PE ligands are typical of P=E double bonds. The P–C distances, at the M052X+D3 level, are 1.830, 1.835, and 1.834 Å for oxide, sulfide, and selenide derivatives, respectively. The E–P–C angles are in the range 113.1°–113.9° for the three compounds. Compared to n-Bu_3PO, one may note that the E–P–C angle and P–C distance only slightly change with E. However, as expected, we observe a lengthening of the P=E bond length. This is accompanied by a reduction in the fundamental frequency for the P=E stretching mode of the ligands, where we compute 558–586 and 494–508 cm^{-1} for P=S and P=Se, respectively, in fair agreement with the measured values (Table 1). For n-Bu_3PS and n-Bu_3PSe, our structural equilibrium parameters represent predictions, since no experimental determinations are available in the literature. They may be used to assign the respective experimental spectra whenever measured.

3 Structures and bonding of tributylphosphine chalcogenides–$ZnCl_2$ complexes

3.1 Equilibrium structures

Figure 1 gives a global view of the equilibrium structure of the [$ZnCl_2$(n-Bu_3PE)$_2$] (E = O, S or Se) complexes. Geometry optimizations were performed using the B3LYP(+D3), PBE0(+D3), and M05-2X(+D3) functionals, along with the 6-311++G** basis set. The main geometrical parameters are given in Table 2, while the full set of Cartesian coordinates for these complexes can be found in the supplementary material. The geometries of the complexes and their ligands were optimized using analytical gradients. The optimizations were unconstrained, and the vibrational frequencies were used to characterize the stationary points as minima (all real positive frequencies). We used several initial configurations for the Zn–E–P angle ranging from 180° up to 90°. The computations converged to the bent Zn–E–P structure as shown in Fig. 1. In particular, we did not obtain structures (even as local minima) where the Zn–E–P angle is linear or quasi-linear, as found for other phosphine oxide organometallic complexes and related compounds (e.g., $Ph_3POAlCl_3$ and $Ph_3POGaCl_3$ [9]). Hence, only π-type complexes seem to be possible for the Zn(II) organometallic compounds considered in the present study (see below). Moreover, these structures agree well with those synthesized recently by some of us [27].

While M052X functional is usually in a fairly good agreement with the most advanced correlated methods

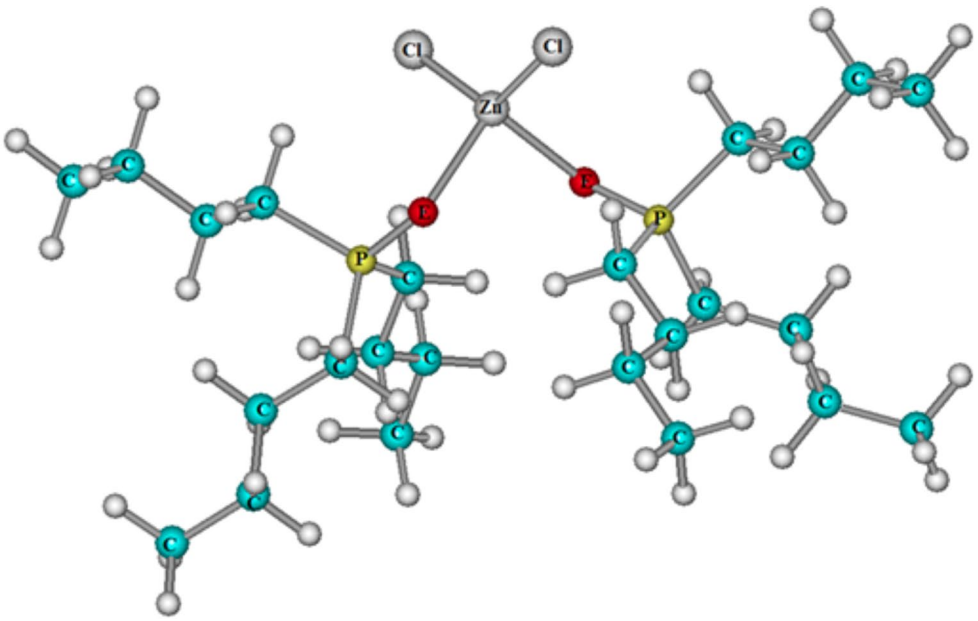

Fig. 1 Optimized equilibrium structure of the complexes $ZnCl_2$(n-Bu_3PE)$_2$ (E = O, S or Se)

Table 2 Main geometrical parameters for the $ZnCl_2$(n-$Bu_3PE)_2$ (E = O, S, Se) complexes as computed using the M05-2X(+D3), PBE0(+D3) and B3LYP(+D3) functionals. Distances are in Å and angles are in degrees. We used the 6-311++G** basis set for these computations. ν(P–E) (E = O, S, Se) is the P=E anharmonic stretching frequency. [a]The full set of data is given in the supplementary material

	M05-2X	M052X+D3	PBE0	PBE0+D3	B3LYP	B3LYP+D3	Exp.[b]
$ZnCl_2$(n-$Bu_3PO)_2$							
P=O	1.535	1.535	1.529	1.531 (1.538)[c]	1.533	1.535	1.515
P–C	1.820	1.819	1.820	1.816 (1.815)[c]	1.834	1.828	1.787
Zn–O	2.019	2.024	2.012	2.040 (2.008)[c]	2.023	2.059	1.980
Zn–Cl	2.263	2.260	2.249	2.230 (2.267)[c]	2.270	2.247	2.238
Zn–O–P	124.1	123.4	128.9	123.5 (127.4)[c]	131.3	124.0	131.0
O–Zn–Cl	104.9	104.3	104.5	104.8 (105.5)[c]	104.7	104.8	107.7
ν(P–O)	1051	1050	1067	1060 (1070)[c]	1059	1049	
$ZnCl_2$(n-$Bu_3PS)_2$							
P=S	2.025	2.024	2.019	2.017	2.033	2.032	2.000
P–C	1.831	1.829	1.828	1.825	1.847	1.838	1.822
Zn–S	2.466	2.467	2.445	2.444	2.490	2.479	2.376
Zn–Cl	2.270	2.270	2.251	2.246	2.265	2.263	2.256
Zn–S–P	100.1	99.9	102.7	100.4	105.0	100.5	109.1
S–Zn–Cl	110.5	110.5	110.3	110.3	109.9	110.1	108.4
ν(P–S)	597	598	600	603	593	593	
$ZnCl_2$(n-$Bu_3PSe)_2$							
P=Se	2.177	2.177	2.176	2.172	2.196	2.192	2.178
P–C	1.831	1.830	1.829	1.827	1.844	1.840	1.823
Zn–Se	2.582	2.542	2.525	2.521	2.581	2.577	2.515
Zn–Cl	2.274	2.289	2.267	2.265	2.290	2.283	2.261
Zn–Se–P	96.8	94.9	96.8	96.4	99.6	95.5	102.4
Se–Zn–Cl	110.3	110.3	112.4	111.2	111.7	110.5	110.6
ν(P–Se)	530	532	529	533	523	530	

[a]Anharmonic frequencies are deduced from the corresponding harmonic ones after using these scaling factors [15]: for M05-2X = 0.9470, PBE0 = 0.9592, B3LYP = 0.9662 for high frequencies and M05-2X = 0.9688, PBE0 = 0.9698, B3LYP = 0.9833 for low frequencies

[b]X-ray structure. Ref. [27]

[c]Values calculated in solvent (chloroform) within the PCM model as implemented in Gaussian 09

for thermochemistry, the reproduction of structural data with this approach is not as satisfactory. Systematic comparisons of all the calculated distances and angles given in Table 2 for the three complexes show that the best overall agreement is provided by PBE0 (without D3) followed by B3LYP, whereas M052X leads almost systematically to the largest errors with respect to experimental data.

Data in Table 2 allow to assess the effects of the dispersion corrections on the equilibrium parameters of complexes [$ZnCl_2$(n-$Bu_3PE)_2$] (E = O, S or Se), indicating that the calculated differences are sensitive to the choice of the DFT functionals. This is particularly noticeable for the bonds involving Zn (i.e., Zn–Cl and Zn–E), because these are more influenced than others by electrostatic and dispersion contributions. These findings are consistent with previous benchmark computations dealing with Zn(II)-organo compounds (e.g., Zn^{2+}-imidazole [28, 29] and Zn^{2+}-triazole [30]). In the following, we will refer to the DFT+D3 values since these should be more reliable.

For [$ZnCl_2$(n-$Bu_3PO)_2$] complex, the distance between P and O is calculated ~ 1.53 Å (Table 2), that is longer than the P=O bond in the isolated ligand, whereas a slightly shorter P–C distance is computed (by 0.01 Å) upon complexation. For the bonds involving Zn(II), we evaluate Zn–O ~ 2.03 Å and Zn–Cl ~ 2.25 Å. For Zn–O–P and O–Zn–Cl angles, we find 123.5° and 104.4°, respectively. For the other two complexes, we compute: P–S ~ 2.02 Å, P–Se ~ 2.17 Å, Zn–S ~ 2.45 Å, Zn–Se ~ 2.53 Å, Zn–S–P ~ 100° and Zn–Se–P ~ 95°. P–C and Zn–Cl distances are close to those given above for $ZnCl_2$(n-$Bu_3PO)_2$. Generally, our geometrical parameters are in close accord with those deduced by X-ray analyses of the recently synthesized [$ZnCl_2$(n-$Bu_3PE)_2$] (E = O, S, Se) compounds [27]. The slight differences between computed and measured ones may be attributed to condensed phase (in experiment) induced modifications compared to gas phase structures (here).

To examine the effect of the solvent on the calculated geometric parameters, we performed additional calculations on

the $ZnCl_2(Bu_3PO)$ complex in chloroform, according to the polarizable continuum model (PCM) by Tomasi and coworkers [31], as implemented in Gaussian 09. The results, obtained at the PBE0+D3 level of theory, are shown in parenthesis in the corresponding column of Table 2. The comparison of the geometric parameters in the gas phase and in the solvent show that only slight variations in the values of bond distances (~0.02 Å) and bond angles (less than 4°) occur. Similarly, in the solvent, we observe only a small increase in the P–O stretching frequency of 10 cm^{-1}. We deduce that the parameters in Table 2 should be also representative, to a similar level of accuracy, of the structure of these complexes in chloroform.

3.2 Binding energies

The strength of the interaction between Zn^{2+} and the ligands in $[ZnCl_2(n\text{-}Bu_3PE)_2]$ (E = O, S, Se) can be quantified after the evaluation of their binding energies (BEs). These quantities are also relevant to investigate the various types of contributions involved in the stabilization of these complexes. Here, BEs are computed after correcting for the basis set superposition error (BSSE), using the Boys–Bernardi scheme: $BE = E_{AB} - (E_A + E_B)$, where E_{AB} is the total electronic energy of the complex, and E_A and E_B are the total electronic energies of the A and B fragments, at the same geometries as in the complex, computed with the full (A + B) basis set.

The BEs for the mono-ligand and bi-ligand complexes from $ZnCl_2$ and n-Bu_3PE (E = O, S, Se) are given in Table 3. In contrast to the geometric equilibrium parameters, this table shows that large deviations can be seen between the values computed with and without inclusion of dispersion corrections and between those obtained using different DFTs. For instance, the inclusion of D3 corrections leads to 1–2, 4–10, and 6–18 kcal mol^{-1} deviations when using M05-2X, PBE0, and B3LYP, respectively. Also, we observe 8–10 kcal mol^{-1} differences between M05-2X, PBE0, and B3LYP. Note that we recently showed, after performing benchmark computations in which several DFT approaches were compared against highly correlated standard [CCSD(T)] and explicitly correlated coupled cluster (CCSD(T)-F12) methods, that the best (i.e., closest to these ab initio methods) estimates of the bonding energies of Zn(II) organo complexes are obtained with the M05-2X+D3 level (see Refs. [29, 30, 32, 33] for more details). Therefore, we consider the M05-2X+D3 BEs for the $ZnCl_2(n\text{-}Bu_3PE)_2$ (E = O, S, Se) complexes as the most accurate predictions.

At the M05-2X+D3/6-311++G** level, we compute BEs of − 51.3, − 49.4 and − 49.5 kcal mol^{-1} for the mono-ligand complex of $ZnCl_2$ with n-Bu_3PE for E = O, S and Se, respectively. These BEs are very similar (differences are less than around 2 kcal mol^{-1}, i.e., in the usual energy range of standard DFT calculations) and relatively small if compared to those computed for the Zn^{2+}-imidazole (~ −180 kcal mol^{-1} [29]) and Zn^{2+}-triazoles (−180 < BE < −140 kcal mol^{-1} [30]) mono-ligand complexes. This is due to the stronger chemical bond that Zn^{2+} forms with nitrogen containing heterocycles in the latter cases. Table 3 shows also that less energy (~ 10 kcal mol^{-1} whatever the chalcogen) is required for binding the second ligand. This reduction in BEs may be related to the less positive charge on Zn^{2+} in $ZnCl_2(n\text{-}Bu_3PE)$ compared to that in bare $ZnCl_2$.

Interestingly, the addition of the second ligand is slightly more discriminating, especially between O and S/Se. Finally, for the reaction $ZnCl_2 + 2\ n\text{-}Bu_3PE = ZnCl_2(n\text{-}Bu_3PE)_2$, the trend is different from the addition of only one ligand, whatever the functional. A less energetic binding from O to S, then a more energetic binding from S to Se is calculated. This tendency is difficult to interpret and may be due to the balance of opposite trends for the different chalcogens.

We also performed a natural bond orbital (NBO) analysis (see Table S5) [34, 35]. Our calculations show that inter- and intra-molecular charge transfers enhance the complex

Table 3 Binding energies ($BE = E_{AB}\text{-}(E_A + E_B)$, BEs in kcal mol^{-1}) of $ZnCl_2(n\text{-}Bu_3PE)_2$ (E = O, S, Se) as computed at the DFT(+D3)/6-311++G** level of theory

	M05-2X	M05-2X+D3	PBE0	PBE0+D3	B3LYP	B3LYP+D3
$A = ZnCl_2$; $B = n\text{-}Bu_3PE$						
E=O	− 50.40	− 51.32	− 43.53	− 47.72	− 39.52	− 46.18
E=S	− 48.45	− 49.39	− 43.55	− 48.62	− 38.05	− 46.32
E=Se	− 48.58	− 49.50	− 44.22	− 49.33	− 38.67	− 47.05
$A = ZnCl_2(n\text{-}Bu_3PE)$; $B = n\text{-}Bu_3PE$						
E=O	− 39.57	− 42.06	− 31.00	− 38.76	− 26.23	− 37.90
E=S	− 36.66	− 38.78	− 29.44	− 37.84	− 22.87	− 36.07
E=Se	− 36.12	− 39.13	− 27.90	− 38.37	− 20.55	− 36.47
$A = ZnCl_2$; $B = 2\ (n\text{-}Bu_3PE)$						
E=O	− 89.34	− 91.22	− 71.58	− 80.55	− 67.31	− 81.76
E=S	− 80.25	− 82.12	− 66.86	− 77.31	− 58.99	− 76.13
E=Se	− 89.72	− 92.57	− 75.34	− 87.04	67.11	− 86.21

stability. The extent of the intra-molecular charge transfer in chalcogen bearing ligands is in the following order: LP(O) to BD*(C–P) > LP(S) to BD*(C–P) > LP(Se) to BD*(C–P), where BD* and LP stand for the 2-center anti-bonding and the 1-center valence lone pair. For S and Se, we observe a stronger metal–ligand interaction that corresponds to a weaker intra-molecular interaction and to a larger charge transfer from Cl ions. The significant enhancement in the S- and Se- than in O-based complexes is due to the weaker back-bonding effects in the O-based ones.

3.3 Frontier molecular orbitals

Figure 2 shows the frontier molecular orbitals of $ZnCl_2(n\text{-}Bu_3PE)_2$ (E = O, S, Se) complexes as calculated at the M05-2X/6-311++G(d,p) level. This figure reveals that the HOMO of $ZnCl_2(n\text{-}Bu_3PO)_2$ is mainly due to the lone pairs of Cl atoms with small contributions from O, whereas those of $ZnCl_2(n\text{-}Bu_3PS)_2$ and $ZnCl_2(n\text{-}Bu_3PSe)_2$ are essentially lone pairs of S and Se, respectively. This figure shows also that the LUMOs are diffuse and expand over the tributylphosphine chalcogenide. Thus, we expect a charge transfer from the E-Zn-Cl part of the complex to the ligands upon HOMO–LUMO orbital interaction.

4 Discussion

Figure 3 displays the unfavorable and favorable interactions between the HOMOs of the $n\text{-}Bu_3P{=}E$ (E = O, S, Se) ligands and the LUMO of bent $ZnCl_2$. The HOMO of the $n\text{-}Bu_3P{=}O$ ligand corresponds mostly to a π* PO bond, where the 2 s and 2p atomic orbitals (AOs) of oxygen have an sp^2 hybridization, whereas the HOMOs of $n\text{-}Bu_3P{=}S$ and $n\text{-}Bu_3P{=}Se$

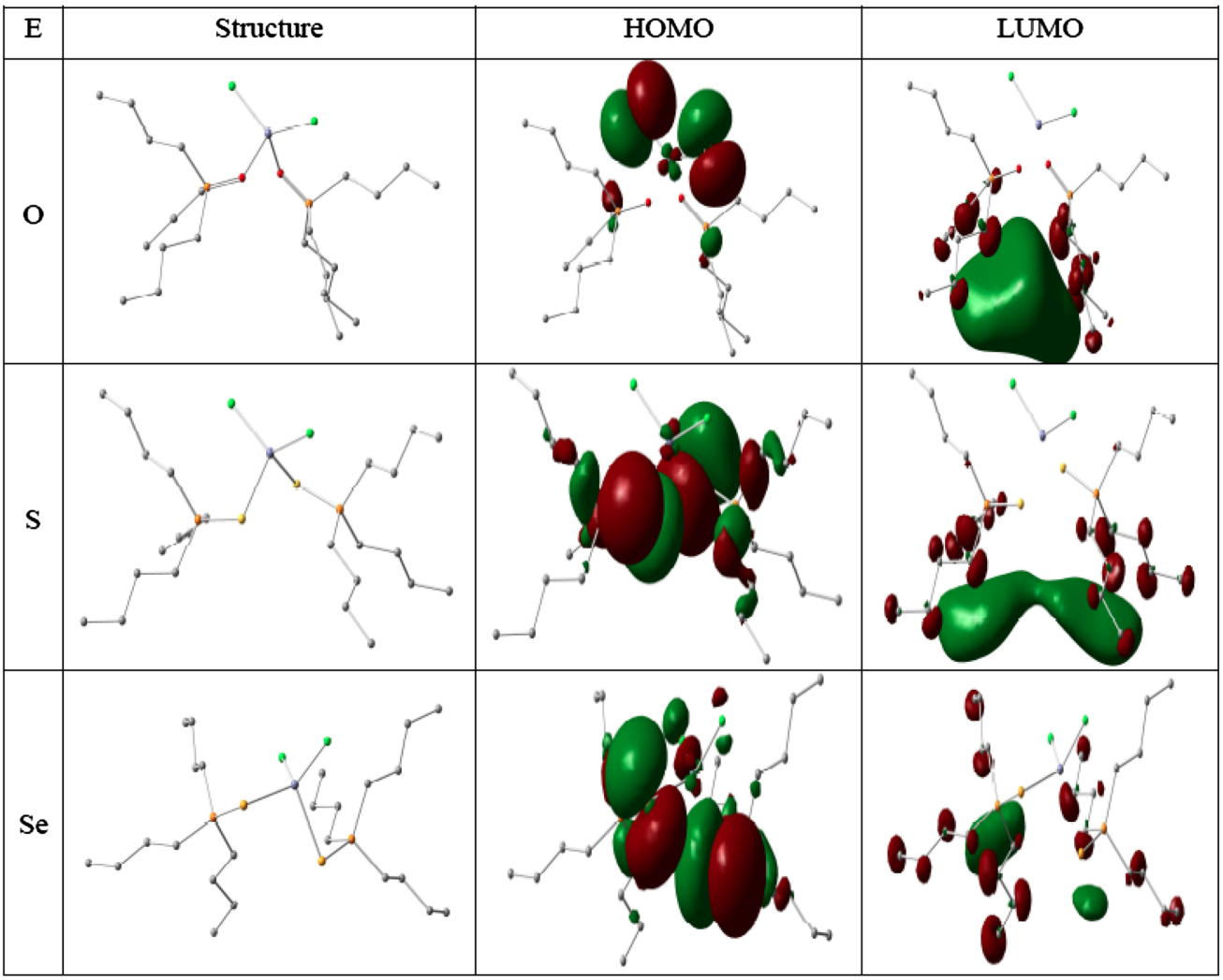

Fig. 2 $ZnCl_2(n\text{-}Bu_3PE)_2$ (E = O, S, Se) complexes frontier molecular orbitals (isosurface density = 0.02 a.u.) as calculated at the M05-2X/6-311++G(d,p) level

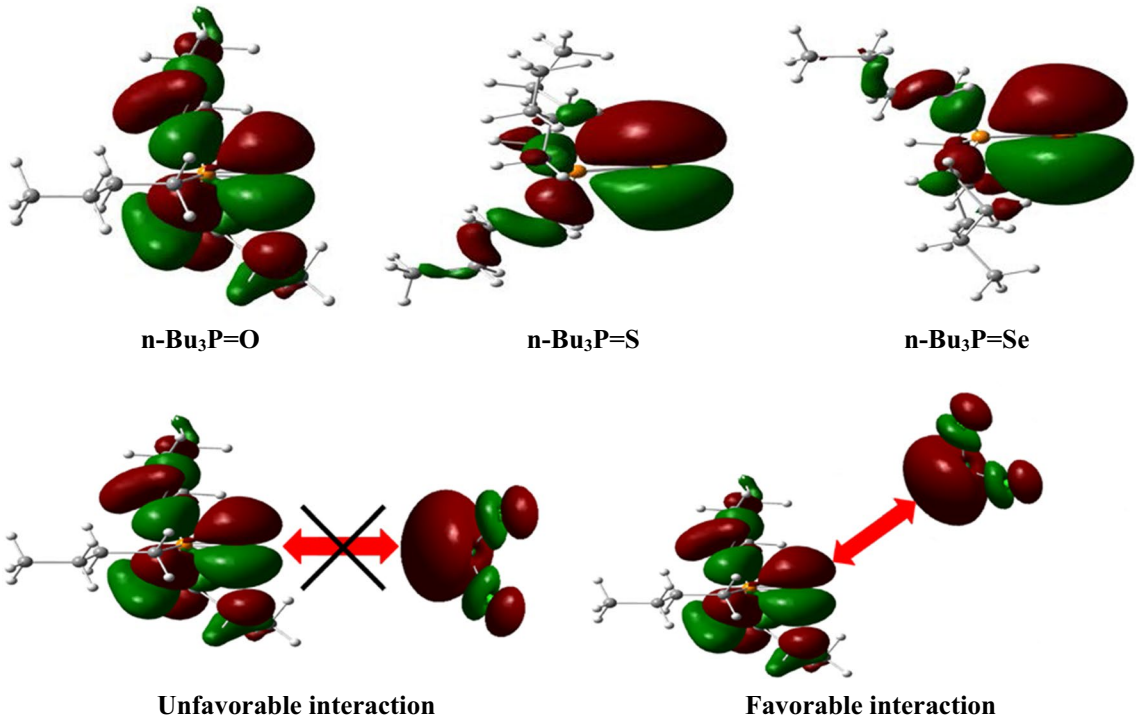

Fig. 3 Upper trace: HOMOs of n-Bu_3P=E (E = O, S, Se). Lower trace: illustration of unfavorable and favorable interactions between the n-Bu_3P=E (E = O, S, Se) HOMOs and the LUMO of bent $ZnCl_2$. These MOs are drawn with an isosurface density = 0.02 a.u. as calculated at the M05-2X/6-311++G(d,p) level

are mostly localized on the chalcogen atom and have more of a lone pair character. Therefore, when going from oxygen to selenium, these molecular orbitals have increasing *p* atomic orbital character and have an influence on the Zn-E-P angle (see Table 2). Similar evolutions of the bond angles are known for other chalcogen-containing molecules. For instance, the in-plane angle around the chalcogen is reduced from 104.48° in H_2O [36], to 92.2° in H_2S [37] and to 90.85° in H_2Se [38]. Moreover, Fig. 3 shows that the ligand-$ZnCl_2$ bond is formed by axial overlap between the HOMOs of the ligands and the $ZnCl_2$ LUMO for bent structures, whereas collinear interactions lead to unfavorable overlap. Indeed, the angle formed by the bonding lobe of these HOMOs with the P=E bond axis is expected to be ~ 120°, ~ 100° and ~ 90° for E = O, S and Se. This simple model fits quite well with the computed Zn-E-P angles, i.e., 123.5°, 100° and 95° for E = O, S, and Se, respectively (Table 2). Therefore, the geometries of the complexes can be easily explained by the favorable interactions between the frontier molecular orbitals of the ligands and those of $ZnCl_2$. This reflects the increasing π-type bonding character of these complexes with the size of the chalcogen.

For isolated P=E and PE^- diatomic anions in their respective electronic ground states, the following interatomic distances were computed at the CAS-ACPF level of theory: $R_e(PO, X^2\Pi) = 1.4886$ Å, $R_e(PS, X^2\Pi) = 1.9148$ Å, $R_e(PSe, X^2\Pi) = 2.0578$ Å, $R_e(PO^-, X^3\Sigma^-) = 1.5496$ Å, $R_e(PS^-, X^3\Sigma^-) = 2.0156$ Å and $R_e(PSe^-, X^3\Sigma^-) = 2.1602$ Å [39]. Thus the addition of an extra electron to the neutral PE diatomic is accompanied by a lengthening of the corresponding internuclear distances. Here similar tendencies are observed upon complexing the n-butyl chalcogenides to $ZnCl_2$. Indeed, the PE distances increase from 1.50 to 1.53 Å for E=O, from 1.97 to 2.02 Å for E=S and from 2.12 to 2.17 Å for E=Se. Interestingly, the PE bond lengths computed for isolated diatomic anions and within the complex almost coincide (Table 2). Thus, upon complexation, the phosphorous-chalcogen bond features more of a single-bond character. For explanation, one may consider back-donation of Zn electrons into the ligand's π* MOs. This contributes to the weakening of the PE bond and, consequently, to its lengthening. According to the electronegativity scale, the excess of negative charge in the E–P bond tends to be localized on the chalcogen atom, resulting in a Zn^+–E^-–P polarization. Again, this is in agreement with the less pronounced double bond character we derive from Wiberg indices for $ZnCl_2$(n-$Bu_3PE)_2$ (E = O, S, Se) (Table 4). These findings further corroborate the π-type bonding scheme for these complexes.

For $ZnCl_2$(n-$Bu_3PO)_2$, the lengthening of the P–O bond during complexation is consistent with the lowering of the P–O stretching frequency for the free and complexed

Table 4 Wiberg indices for n-Bu_3P=E (E = O, S, Se) compounds and for their complexes with $ZnCl_2$

	n-Bu_3P=E			$ZnCl_2$(n-$Bu_3PE)_2$		
E	O	S	Se	O	S	Se
W(P=E)	1.2	1.370	1.312	1.0	1.18	1.15
W(Zn–E)	–	–	–	0.21	0.41	0.49

ligands, where a decrease of 76 cm^{-1} is computed for ν(P–O), whereas we observe an increase in ν(P–S) and ν(P–Se) frequencies of 22 and 32 cm^{-1} upon complexation. This increase in the P–E stretching frequencies, which is not consistent with the lengthening of the P–E bonds and with the Wiberg indices of Table 4, can be possibly explained with the particular mechanism through which back-donation of electronic charge from Zn to the ligands takes place in these complexes. Instead of involving π^* molecular orbitals on the ligands, here back-donation exploits contributions from the *p* atomic orbitals of S (3*p* and 4*p*) and of Se (4*p* and 5*p*). Evidence for this mechanism, which is not active in the oxygen's case, is supported by the results of natural population analysis (NPA). For instance, we compute for sulfur an increase of 0.08 *e* in the natural population of the 3*p* and 4*p* orbitals upon complexation, while a loss of 0.06 *e* in the natural population of the same orbitals is computed for phosphorous. Similar results are obtained for the selenium-based ligand. The extent of this back-donation mechanism is not overwhelming, but is sufficient to account for the slight increase in the P-E stretching vibrational frequencies occurring for the heavier chalcogenides. In addition to this, we note that the increase in the harmonic vibrational frequencies is not that large and could also be due to different mixing with the close-lying C–C–C bending modes on the t-Bu units attached to the ligands, which contribute to the P-E stretching mode of both free and complexed structures.

5 Conclusions

In this work, we have optimized the structures of three complexes of $ZnCl_2$ with tributylphosphine chalcogenides, containing O, S, or Se, using DFT calculations based on different choices of energy functionals, with and without inclusion of empirically determined corrections, at the GD3 level of theory, for the dispersion interactions.

Our calculations show a systematic increase in the P–E bond length in these complexes, accompanied by a decrease in Zn–E–P angle, when passing from oxygen- to selenium-based ligands. We have shown that DFT calculations are a useful supporting tool for such investigations, since the compared analysis of data from empirical and first-principles approaches can help, in favorable cases, to overcome the limitations of both experiment and theory.

The role of various types of covalent and non-covalent interactions within these complexes is discussed in terms of the changes in the vibrational frequencies for some selected normal modes upon complexation, and by performing NBO and MO analysis.

We conclude that, in order to establish the nature of ligand–metal bonding (σ- or π-type mainly) within the complex, one can focus almost exclusively on the variations of the P–E bond length and of the M–P–E bond angle upon complexation. Also, we show that R_3PE–$ZnCl_2$ (E = O, S, Se) do not fall into this category and that they exhibit a $P–E^-$ character due to the charge transfer from the atoms surrounding the chalcogen to the chalcogen within the complex. A third type of bonding is proposed here for the first time. Therefore, our calculations suggest that the bonding within already known organophosphine chalcogenides complexes with metallic ions should be reinvestigated in light of this new model.

Acknowledgements We are grateful to the Tunisian Ministry of High Education and Scientific Research for financial support (LR99ES14) of this research. M. P. thanks the Department of Science and Technology-Science and Engineering Research Board (DST-SERB) of India for the financial support for early career research award (Grant number: ECR/2017/000891).

Compliance with ethical standards

Conflict of interest There are no conflicts of interest to declare.

References

1. Mikulski CM, Skryantz JS, Karayannis NM, Pytlewski LL, Gelfand LS (1978) Inorg Chim Acta 27:69–73
2. Karayannis NM, Mikulski CM, Pytlewski LL (1971) Inorg Chim Acta Rev 5:69
3. Cotton FA, Bannister E (1960) J Chem Soc 1873–1877
4. Goodgame DML, Cotton FA (1961) J Chem Soc 2298:3735
5. Brodie AM, Hunter SH, Rodley GA, Wilkins CJ (1968) J Inorg Chim Acta 2:195
6. Karayannis NM, Mikulski CM, Pyrlewski LL (1977) J Inorg Chim Acta Rev 5:69
7. Qu L, Peng Z, Peng X (2001) Nano Lett 1:333–337
8. Jasieniak J, Bullen C, Van EJ, Mulvaney P (2005) J Phys Chem B 109:20665–20668
9. Burford N, Royan BW, Spence REvH, Cameron TS, Linden A, Rogers RD (1990) J Chem Soc Dalton Trans 1521 and refs therein
10. Burford N, Royan BW, Spence REvH, Rogers RD (1990) J Chem Soc Dalton Trans 2111–2117
11. Bania K, Barooah N, Baruah JB (2007) Polyhedron 26:2612–2620

12. Afzall M, Crouch D, Malik MA, Motevalli M, O'Brien P, Park J-H, Woollins JD (2004) Eur J Inorg Chem 171–177
13. Waters J, Crouch DJ, Raftery J, O'Brien P (2004) Chem Mater 16:3289
14. Chivers T, Ritch JS, Robertson SD, Konu J, Tuononen HM (2010) Acc Chem Res 43:1053
15. Laury ML, Carlson MJ, Wilson AK (2012) J Comput Chem 33:2380–2387
16. Hilliard CR, Bhuvanesh N, Gladysz JA, Blumel Janet (2012) Dalton Trans 41:1742
17. Grim SO, Walton ED, Satek LC (1980) Can J Chem 58:1476
18. Zhao Y, Truhlar DG (2005) Phys Chem Chem Phys 7:2701–2705
19. Adamo C, Barone V (1999) J Chem Phys 110:6158–6170
20. Perdew JP, Ernzerhof M, Burke K (1996) J Chem Phys 105:9982–9985
21. Ernzerhof M, Scuseria GE (1999) J Chem Phys 110:5029–5036
22. Becke AD (1993) J Chem Phys 98:5648–5652
23. Becke AD (1988) Phys Rev A 38:3098
24. Lee C, Yang W, Parr RG (1988) Phys Rev B37:785–789
25. Grimme S, Antony J, Ehrlich S, Krieg H (2010) J Chem Phys 132:154104
26. Frisch MJ, Trucks GW, Schlegel HB, Scuseria GE, Robb MA, Cheeseman JR, Scalmani G, Barone V, Mennucci B, Petersson GA, Nakatsuji H, Caricato M, Li X, Hratchian HP, Izmaylov AF, Bloino J, Zheng G, Sonnenberg JL, Hada M, Ehara M, Toyota K, Fukuda R, Hasegawa J, Ishida M, Nakajima T, Honda Y, Kitao O, Nakai H, Vreven T, Montgomery JA Jr, Peralta JE, Ogliaro F, Bearpark M, Heyd JJ, Brothers E, Kudin KN, Staroverov VN, Kobayashi R, Normand J, Raghavachari K, Rendell A, Burant JC, Iyengar SS, Tomasi J, Cossi M, Rega N, Millam JM, Klene M, Knox JE, Cross JB, Bakken V, Adamo C, Jaramillo J, Gomperts R, Stratmann RE, Yazyev O, Austin AJ, Cammi R, Pomelli C, Ochterski JW, Martin RL, Morokuma K, Zakrzewski VG, Voth GA, Salvador P, Dannenberg JJ, Dapprich S, Daniels AD, Farkas O, Foresman JB, Ortiz JV, Cioslowski J, Fox DJ (2009) Gaussian 09W Revision A. 02, Gaussian, Inc., Wallingford, CT
27. Gouid Z, Sanhoury MAK, Ben Said R, Carpenter-Warren CL, Slawin AMZ, Ben Dhia MT, Derek Woollins J, Boughdiri S (2017) J Coord Chem 70:3859–3870
28. Piquemal JP, Marquez A, Parisel O, Giessner-Prettre C (2005) J Comput Chem 26:1052
29. Boussouf K, Boulmene R, Prakash M, Komiha N, Taleb M, Mogren Al-Mogren M, Hochlaf M (2015) Phys Chem Chem Phys 17:14417
30. Dahmani R, Ben Yaghlane S, Boughdiri S, Mogren Al-Mogren M, Prakash M, Hochlaf M (2018) Spectrochim Acta A Mol Biomol Spectrosc 193:375–384
31. Miertus S, Scrocco E, Tomasi J (1981) Chem Phys 55:117
32. Boussouf K, Khairat T, Prakash M, Komiha N, Chambaud G, Hochlaf M (2015) J Phys Chem A 119:11928–11940
33. Boulmene R, Boussouf K, Prakash M, Komiha N, Al-Mogren MM, Hochlaf M (2016) ChemPhysChem 17:994
34. Weinhold F, Carpenter JE (1988) In: Naaman R, Vager Z (eds) The structure of small molecules and ions. Plenum, New York, pp 227–236
35. Reed AE, Curtiss LA, Weinhold F (1988) Chem Rev 88:899–926
36. Császár AG, Czakó G, Furtenbacher T, Tennyson J, Szalay V, Shirin SV, Zobov NF, Polyansky OL (2005) J Chem Phys 122:214305
37. Chang JH, Huzayyin A, Lianc K, Dawson F (2015) Phys Chem Chem Phys 17:588
38. Oka T, Morino Y (1962) J Mol Spectrosc 8:300–314
39. Kalcher J (2002) Phys Chem Chem Phys 4:3311–3317